AFRL-AFOSR-UK-TR-2018-0038

High Power Microwave Low contrast surface artificial materials

Alan Phelps
UNIVERSITY OF STRATHCLYDE VIZ ROYAL COLLEGE OF SCIENCE & TECHNOLOGY
16 RICHMOND STREET
GLASGOW, G1 1XT
GB

08/16/2018
Final Report

DISTRIBUTION A: Distribution approved for public release.

Air Force Research Laboratory
Air Force Office of Scientific Research
European Office of Aerospace Research and Development
Unit 4515 Box 14, APO AE 09421

REPORT DOCUMENTATION PAGE

Form Approved
OMB No. 0704-0188

1. REPORT DATE *(DD-MM-YYYY)*
16-08-2018

2. REPORT TYPE
Final

3. DATES COVERED *(From - To)*
15 Dec 2012 to 14 Dec 2017

4. TITLE AND SUBTITLE
High Power Microwave Low contrast surface artificial materials

5a. CONTRACT NUMBER

5b. GRANT NUMBER
FA8655-13-1-2132

5c. PROGRAM ELEMENT NUMBER
61102F

6. AUTHOR(S)
Alan Phelps, Adrian Cross

5d. PROJECT NUMBER

5e. TASK NUMBER

5f. WORK UNIT NUMBER

7. PERFORMING ORGANIZATION NAME(S) AND ADDRESS(ES)
UNIVERSITY OF STRATHCLYDE VIZ ROYAL COLLEGE OF SCIENCE & TECHNOLOGY
16 RICHMOND STREET
GLASGOW, G1 1XT GB

8. PERFORMING ORGANIZATION REPORT NUMBER

9. SPONSORING/MONITORING AGENCY NAME(S) AND ADDRESS(ES)
EOARD
Unit 4515
APO AE 09421-4515

10. SPONSOR/MONITOR'S ACRONYM(S)
AFRL/AFOSR IOE

11. SPONSOR/MONITOR'S REPORT NUMBER(S)
AFRL-AFOSR-UK-TR-2018-0038

12. DISTRIBUTION/AVAILABILITY STATEMENT
A DISTRIBUTION UNLIMITED: PB Public Release

13. SUPPLEMENTARY NOTES

14. ABSTRACT
Two dimensional (2D) periodic surface lattices (PSLs) constructed on the inner surface of a cylindrical, highly overmoded interaction region have been shown to provide a route to achieving an eigenmode that can be excited with an electron beam, resulting in a microwave source with a cavity diameter to wavelength ratio much larger than unity. The project combined analytical theory, numerical modelling, component design, construction and operation of an experiment. Two different methods were used to manufacture the two different types of 2D PSL. The first used electrochemical deposition of copper on an aluminum former with the aluminum subsequently removed by dissolving in strong alkali solution and the second used a 3D printing (additive manufacturing) technique. A water-cooled 1.8 T electromagnet solenoid provided the guide field for the electron beam. In the initial experiments 134 kW of mm-wave output was measured in W-band. The 2D PSL principle employed is independent of frequency and has the capability of higher output powers, as a consequence of achieving mode selectivity and control in large, highly-overmoded structures.

15. SUBJECT TERMS
EOARD, metamaterials, high power sources

16. SECURITY CLASSIFICATION OF:			17. LIMITATION OF ABSTRACT	18. NUMBER OF PAGES	19a. NAME OF RESPONSIBLE PERSON
a. REPORT	b. ABSTRACT	c. THIS PAGE			LOCKWOOD, NATHANIEL
Unclassified	Unclassified	Unclassified	SAR		19b. TELEPHONE NUMBER *(Include area code)* 011-44-1895-616005

Standard Form 298 (Rev. 8/98)
Prescribed by ANSI Std. Z39.18

High Power Microwave Low Contrast Surface Artificial Materials

GRANT: FA8655-13-1-2132

FINAL REPORT

1st March 2018

Principal Investigator:

Alan Phelps

University of Strathclyde, Glasgow, Scotland, UK

Period of Performance: 15 Dec 2012 to 14 Dec 2017

TABLE OF CONTENTS

1. Abstract

Two dimensional (2D) periodic surface lattices (PSLs) constructed on the inner surface of a cylindrical, highly overmoded interaction region have been shown to provide a route to achieving an eigenmode that can be excited with an electron beam, resulting in a microwave source with a cavity diameter to wavelength ratio much larger than unity. The project consisted of a combination of analytical theory, numerical modelling, component design, construction and operation of an experiment.

Two different methods were used to manufacture the two different types of 2D PSL. The first method used electrochemical deposition of copper on an aluminum former with the aluminum subsequently removed by dissolving in strong alkali solution. The second method used a 3D printing (additive manufacturing) technique resulting in a silver/chromium alloy 2D PSL. A water-cooled 1.8 T electromagnet solenoid was used to provide the guide field for the electron beam. In the initial experiments 134 kW of millimeter-wave output was measured in W-band.

The 2D PSL principle employed is independent of frequency and provides the capability of providing higher output powers from microwave and millimeter-wave sources, for any given frequency, as a consequence of achieving mode selectivity and control in large, highly-overmoded interaction structures.

2. Introduction

High power microwave and millimeter-wave sources have a number of important defense applications, that include radio frequency (RF) directed energy weapons (DEW) and high power radars. The subject of this report is a combined theoretical, numerical and experimental study of low contrast surface artificial materials in high power microwave sources, with the ultimate aim of improving the scaling of output power as a function of operating frequency for microwave sources. The work described in this report was carried out during the period of years when the MURI 'Transformational Electromagnetics', co-ordinated by Edl Schamiloglu, was running in the USA. The support of this research award enabled the University of Strathclyde group to participate as a UK satellite member of this MURI.

The types of microwave sources that have been the focus of this study are known as "slow wave" sources, in contrast to "fast wave" sources. In a "fast wave" source the electromagnetic (EM) wave travels faster than the electron beam, that transfers its energy to the wave, whereas in a "slow wave" source the electron beam travels faster than the electromagnetic wave. The "slow wave" interaction that occurs in microwave sources such as traveling wave tubes (TWTs) and backward wave oscillators (BWOs) can also be understood as a Cherenkov interaction. Cherenkov radiation occurs when charged particles propagate in or near a medium capable of supporting EM waves whose axial phase velocity can be slightly less than the drift velocity of the electrons so that its dispersion is close to intersecting that of the electron beam at the desired source frequency. Coupling occurs between the space charge wave (electron bunches) of the electron beam and the electric field components of the wave orientated along the direction of the particle drift. The space charge wave originates from modulation of the electrons' velocities by the EM field which leads to the formation of spatial bunches in the electron stream resulting in generation of the electromagnetic wave if decelerated. The essential coupling between the cross sectional diameter of the slow wave structure and the frequency results in a rapid decline in the power handling capability.

The novelty of the work reported here is the circumvention of these limitations by combining the novel capability of two dimensional (2D) surface periodic lattices to regulate the wave dispersion in large volumes (i.e large compared to the wavelength). This can lead to the observation of backward and forward slow waves and can thus be used to create new millimeter and sub-millimeter wave Cherenkov radiation sources. Due to the detailed regulation of the wave dispersion, combined with the distributed nature of the structures, these sources can be inherently oversized and overmoded, enabling the development of high power, Cherenkov oscillators.

Cherenkov sources can be designed using dielectric lined waveguides, that contain an insulating layer of dielectric material on the inner wall of the hollow waveguide through which the electron beam is passed. The disadvantage of using such insulating dielectric liners is that surface charge can be deposited from the electron beam on the liner surface and this can subsequently affect the electron beam propagation.

One approach to overcoming this disadvantage is by the use of a structured (usually corrugated) metallic conducting wall that naturally conducts away any deposited surface charge, as well as having good thermal conduction properties to support high power operation. While for DC currents this structured metallic wall presents a low resistance path, for the EM wave the structured wall can be designed to present a relatively high impedance. Up to this point what has been introduced is essentially a conventional slow-wave device using a one dimensional corrugated structure as in conventional BWOs.

The novelty of the present work is that while preserving the above essential advantages, a more complex two dimensional spatial modulation is applied to the inner conducting metallic wall of the interaction structure. This 'metadielectric' surface is designed to support and couple 4 waves, consisting of two counter-propagating azimuthally propagating waves and two counter-propagating axially propagating waves. In the conventional one dimensional corrugated structures the cross-sectional area of the interaction structure needs to be limited, so that only the lowest order modes propagate in order to retain single mode operation and thereby obtain reasonable efficiency. By using the mode coupling facilitated by the 2D surface structure, also known as a periodic surface lattice (PSL), an eigenmode can be formed even in a much larger cross-sectional area interaction structure. This eigenmode can then be relatively efficiently driven by an electron beam, even in such highly overmoded structures. The benefit resulting from using this 2D PSL structure is that the significant parameter of the ratio of the diameter, D, of the interaction region to the EM wavelength, λ, can be increased from $D/\lambda \sim 1$ to $D/\lambda \sim 3$ or even to much higher values. Since the cross-sectional area increases as the square of this parameter, it can be appreciated that this opens up the path to higher output powers at a given output wavelength, than in the conventional slow-wave source scaling of output power as a function of wavelength.

The principle is applicable at any wavelength. Our work has aimed at proving the principle in the ∼100GHz region, because this has required both relatively modest sized power supplies and a compact interaction region. The principle is equally applicable at 10 GHz or 1 GHz, although to fully exploit the output capabilities at these longer wavelengths much larger power supplies combined with a large volume interaction structure are required.

3. Theory

The PSL's eigenfield for the case of an oversized cylindrical PSL can be described as a superposition of a well-defined $TM_{0,T}$ volume field and high order $TM_{\overline{m},n}$ surface fields. This theory is also applicable to planar PSLs based on the assumption that the mean radius of the cylinder r_0 is large in comparison to the operating wavelength ($r_0 \gg \lambda$), which has been made throughout this analysis. Lattice synchronization is obtained by launching a near cut-off, symmetric $TM_{0,T}$ volume mode (with a uniform longitudinal field) through the structure, or in the case of planar geometry, by exciting a Fabry-Perot standing wave that exists due to scattering of the surface currents. The cylindrical PSL can be substituted for a smooth waveguide with a fictitious magnetic surface current $\underline{j}_m$ in place of the corrugation to describe field coupling or scattering.

From Maxwell's curl equations, $\nabla^2 \underline{H} = -\omega^2 \varepsilon\mu\, \underline{H} + i\omega\varepsilon \underline{j}_m$ where $\underline{\nabla} = \underline{x}_0 \nabla_x + \underline{y}_0 \nabla_y + \underline{z}_0 \nabla_z$ is the Cartesian gradient operator, valid when $r_0 \gg \lambda_{op}$ and providing the corrugation Δr is suitably shallow $\left(\Delta r \ll \lambda_{op}\right)$ the PSL's eigenfield can be described as a superposition of waveguide modes (where the volume and surface modes have real and imaginary transverse wavenumbers respectively). The transverse electric $\underline{E}$ and magnetic $\underline{H}$ fields are expanded as a sum of the possible waveguide modes, allowing the field inside the finite cylinder to be described as a slow wave envelope $C_q(z)$ filled with fast varying terms.

$$\underline{H} = \sum_q \nabla^2 (C_q(z) \underline{H}_q) = -\omega^2 \varepsilon\mu \sum_q C_q(z) \underline{H}_q + i\omega\varepsilon \underline{j}_m \qquad (1)$$

The total power transmitted through the structure is defined by integrating the Poynting vector ${}^1/_2\left(\underline{E} \times \underline{H}^*\right)$ over the cylindrical cross section. This treatment is restricted to consider only the near cut-off volume mode ($\omega \approx \omega_0^v$) for which $k_z \to 0$ and $\lambda_z \to \infty$. In the case of a planar system, the structure is assumed to be infinitely large and edge effects are neglected. In practice, however, some detuning from the ideal situation where $\omega = \omega_0^v$ exists due to the structure's finite length. $\underline{E} \times \underline{H}^*$ is implicitly defined by multiplying both sides of Eq.(1) by the complex conjugate of the transverse magnetic cut-off mode ($\underline{H}_{q'}^*$). Separating ∇^2 into its transverse and longitudinal components and substituting the Helmholtz equation $\nabla_\perp^2 \underline{H}_q \pm \frac{(\omega_0^q)^2}{c^2} \underline{H}_q = 0$ for the localized volume "$+$" and surface "$-$" fields into $\underline{H}_{q'}^* \nabla_z^2 \sum_q C_q(z) \underline{H}_q + \underline{H}_{q'}^* \nabla_\perp^2 \sum_q C_q(z) \underline{H}_q + \omega^2 \underline{H}_{q'}^* \sum_q C_q(z) \underline{H}_q = i\omega\varepsilon \underline{j}_m \underline{H}_{q'}^*$ gives

$$\underline{H}_{q'}^{*}\sum_q \nabla_z^2 C_q(z)\underline{H}_q + \underline{H}_{q'}^{*}\sum_q C_q(z)\left(-\frac{{\omega_0}^2}{c^2}\right)\underline{H}_q + \omega^2 \underline{H}_{q'}^{*}\underline{H}_q = i\omega\varepsilon \underline{j}_m \underline{H}_{q'}^{*}$$
(2)

where q' denotes the near-cut off volume mode. Imposing the orthogonality condition $\int_{S\perp} \underline{H}_q \underline{H}_{q'}^{*} = 0$ if $q \neq q'$ and integrating around the waveguide's circular cross-section gives the normalized wave equation. Small diffractive and Ohmic losses are considered by introducing detuning parameters. The detuning between the volume mode ω_0^v and cavity eigenmode ω is $\frac{(\omega^2-\omega_0^2)}{c^2}$ while the detuning between volume and surface modes is $\Delta = \omega_0^v - \omega_0^s \cong k_z^v$. Satisfying the Bragg resonance condition $\bar{k}_z = k_z^s - k_z^v$ for the localized $(k_z^v \cong 0)$ $TM_{0,T}$ mode, requires that $\omega_B = \omega_0^s$. We define the Bragg detuning $\hat{\delta} = \frac{\omega_B - \bar{\omega}_0}{c^2}$ in terms of the mean angular frequency, $\bar{\omega}_0 = \frac{\omega_0^v + \omega_0^s}{2}$ and incorporate $\hat{\delta}$ into the normalized wave equation.

$$\nabla_z^2 C_q^{v,s}(z) \pm \omega\hat{\delta} C_q^{v,s}(z) + \frac{\bar{\omega}_0\Delta}{c^2} C_q^{v,s}(z) = N_{v,s}\oint \underline{j}_m \underline{H}_{q'}^{*}\, d\sigma \qquad (3)$$

$N_{v,s} = \frac{i\omega\varepsilon}{\oint_{S\perp} \underline{H}_q \underline{H}_{q'}^{*} d\varphi}$ is the wave norm for the volume (v) and surface (s) modes.

Due to the structure's periodicity, it is possible to express the slowly varying surface field as a complex Fourier series of the form $C_q^s(z) = \sum_{n_s=-\infty}^{\infty} B_{n_s}(z) e^{in_s\bar{k}_z z}$ where B_{n_s} is the amplitude of the surface field's n_s harmonic. Likewise, the volume field can be written as a complex Fourier expansion using the approximation $k_{z,v} \cong \bar{k}_z = 2\pi/d_z$ which equates the volume field's longitudinal wavenumber to that of the structure and corresponds to the case of coherent, coupled eigenmode formation i.e. minimal detuning. Evaluating the second order partial differential terms and substituting into Eq.(3) yields wave equations for the volume Eq.(4a) and surface Eq.(4b) modes.

$$\sum_{n_v}\left(e^{in_v\bar{k}_z z}\frac{\partial^2 A_{n_v}(z)}{\partial z^2} - 2in_v\bar{k}_z e^{in_v\bar{k}_z z}\frac{\partial A_{n_v}(z)}{\partial z} - {n_v}^2{\bar{k}_z}^2 A_{n_v}(z)e^{in_v\bar{k}_z z}\right) + \omega\hat{\delta}\left(\sum_{n_v} A_{n_v}(z)\, e^{in_v\bar{k}_z z}\right)\frac{\bar{\omega}_0\Delta}{c^2}\left(\sum_{n_v} A_{n_v}(z)e^{in_v\bar{k}_z z}\right) = N_v\oint \underline{j}_m \underline{H}_{q'}^{*}\, d\sigma$$
(4a)

$$\sum_{n_s}\left(2in_s\bar{k}_z e^{in_s\bar{k}_z z}\frac{\partial B_{n_s}(z)}{\partial z} - n_s^2{\bar{k}_z}^2 B_{n_s}(z)e^{in_s\bar{k}_z z} + e^{in_s\bar{k}_z z}\frac{\partial^2 B_{n_s}(z)}{\partial z^2}\right) - \omega\hat{\delta}\left(\sum_{n_s} B_{n_s}(z)\, e^{in_s\bar{k}_z z}\right) + \frac{\bar{\omega}_0\Delta}{c^2}\left(\sum_{n_s} B_{n_s}(z)e^{in_s\bar{k}_z z}\right) = N_s\oint \underline{j}_m \underline{H}_{q'}^{*}\, d\sigma \qquad (4b)$$

To evaluate the right-hand side of Eq.(4a, b) we must define $\underline{j_m}\underline{H}_q^*$. A cylindrical PSL with sinusoidal corrugation $l = r_0 + \Delta r cos\bar{m}\varphi cos\bar{k}_z z$ and $\bar{m}$ azimuthal variations is equivalent to a smooth cylindrical waveguide when the magnetic surface current boundary condition $\underline{j_m} = \underline{n} \times \left(\overline{\nabla}\left(l\underline{E}\ \underline{n}\right)\right) + i\omega l\underline{n} \times \left[\underline{n} \times \underline{\mathrm{H}}\right]$ is satisfied. For planar geometry, $\bar{m}\varphi$ is substituted with $\bar{k}_y y$ where $\bar{k}_y = 2\pi/d_y$. Enforcing this condition gives $\underline{j_m}\underline{H}_q^* = i\omega l(z,\varphi)\left(\underline{E}_{q,n}\underline{E}_{q,n}^* + \underline{H}_{q,\tau}\underline{H}_{q,\tau}^*\right)$ where $\underline{E}_{q,n}$ and $\underline{H}_{q,\tau}$ are the normal electric and tangential magnetic field components with complex conjugates $\underline{E}_{q,n}^*$ and $\underline{H}_{q,\tau}^*$. In the case of a $TM_{0,T}$ volume mode (with no normal electric field component) $\underline{E}_{q,n} = 0$. Separating $\underline{H}_{q,\tau}$ into its volume and surface field constituents $\underline{H}_{q,\tau} = \underline{H}_{q,\tau}^v(r)C_q^v(z) + \underline{H}_{q,\tau}^s(r,\varphi)C_q^s(z)$ and expanding to include the full set of eigenmodes gives

$$\underline{j_m}\underline{H}_q^* = i\omega\left[r_0 + \frac{\Delta r}{4}\left(e^{i\bar{m}\varphi} + e^{-i\bar{m}\varphi}\right)\left(e^{i\bar{k}_z z} + e^{-i\bar{k}_z z}\right)\right]\underline{H}_{q,\tau}^{*,v}\left(\underline{H}_{q,\tau}^v(r)\sum_2 C_q^v(z) + \underline{H}_{q,\tau}^s(r)cosm_s\varphi\sum_{n_s} B_{n_s}(z)e^{in_s\bar{k}_z z}\right) \quad (5)$$

The $\underline{j_m}\underline{H}_q^*$ term is now integrated over the cylindrical cross section $d\sigma$, where $N_{v,s}' \oint \underline{j_m}\underline{H}_{q,\tau}^{*(v,s)}\, d\sigma = N_{v,s}' \int_0^{2\pi} r\left(\underline{j_m}\underline{H}_q^*\right)\Big|_{r=r_0} d\varphi$ and $N_{v,s}' = i\omega N_{v,s}$. One of the necessary criteria for volume and surface mode coupling is $\oint \underline{j_m}\underline{H}_q^*\, d\sigma \neq 0$. This requirement is satisfied by averaging over the period of fast oscillations from 0 to 2π, neglecting exponential (oscillating) terms that would otherwise integrate to zero. The fundamental volume field harmonic $(n_v = 0)$ is first described in the form $\oint \underline{j_m}\underline{H}_q^*\, d\sigma = r_0^2 N_v' \int_0^{2\pi} r\,(I)|_{r=r_0} d\varphi$ where *I* is the integrand, composed of four terms

(1) $r_0\underline{H}_{q,\tau}^{*v}(r)\underline{H}_{q,\tau}^v(r)\sum_2 C_q^v(z)$
(2) $r_0\underline{H}_{q,\tau}^{*v}\underline{H}_{q,\tau}^s(r)cosm_s\varphi\sum_{n_s} B_{n_s}(z)e^{in_s\bar{k}_z z}$
(3) $r_0\frac{\Delta r}{4}\left(e^{i\bar{m}\varphi} + e^{-i\bar{m}\varphi}\right)\left(e^{i\bar{k}_z z} + e^{-i\bar{k}_z z}\right)\underline{H}_{q,\tau}^{*v}\underline{H}_{q,\tau}^v(r)\sum_2 C_q^v(z)$
(4) $\frac{\Delta r}{4}\left(e^{i\bar{m}\varphi} + e^{-i\bar{m}\varphi}\right)\left(e^{i\bar{k}_z z} + e^{-i\bar{k}_z z}\right)\underline{H}_{q,\tau}^{*v}\underline{H}_{q,\tau}^s(r)cosm_s\varphi\sum_{n_s} B_{n_s}(z)e^{in_s\bar{k}_z z}$

Terms 2 and 4 demonstrate scattering and potential coupling of volume and surface fields. The geometric parameter $\frac{\Delta r}{r_0}$ is closely linked to the coupling coefficient. Discarding terms 2 and 3 (which integrate to zero after averaging over the fast oscillation terms) and employing the trigonometric identity $cosm_s\varphi = 1/2\left(e^{im_s\varphi} + e^{-im_s\varphi}\right)$ gives

$$\underline{j_m}\underline{H}_q^* = r_0^2 N_v' \int_0^{2\pi} \Big(\underline{H}_{q,\tau}^{*v}(r_0) \underline{H}_{q,\tau}^{v}(r_0) \textstyle\sum_2 C_q^v(z) + \frac{\Delta r}{8 r_0} \underline{H}_{q,\tau}^{*v}(r_0) \underline{H}_{q,\tau}^{s}(r_0) \left(e^{i\bar{k}_z z} + e^{-i\bar{k}_z z} \right) \left(e^{i\bar{m}\varphi} + e^{-i\bar{m}\varphi} \right) \left(e^{i m_s \varphi} + e^{-i m_s \varphi} \right) \textstyle\sum_{n_s} B_{n_s}(z) e^{i n_s \bar{k}_z z} \Big) \Big|_{r=r_0} d\varphi \qquad (6)$$

A non-trivial result is obtained only when $m_s = \bar{m}$, forcing the fast oscillation terms to vanish. Based on the azimuthal Bragg condition, $\bar{m} = m_v + m_s$, we establish that $m_v = 0$, justifying the role of the azimuthally symmetric $TM_{0,T}$ volume mode. The remaining fast oscillation terms are eliminated when $n_s = \pm 1$. Until now, only the fundamental harmonic of the volume field has been considered. For completeness, and to provide a more thorough mathematical description of the possible scattering processes, the Fourier expansion of both fields is included, allowing different low order values of n_v and n_s to be explored. We follow a similar procedure to that above, now multiplying $\underline{j_m}\underline{H}_q^*$ by $e^{-i\bar{k}_z z n_{v,s}}$ to describe possible coupling mechanisms involving the $n_{v,s} = 0$ and $n_{v,s} = \pm 1,2$ field harmonics. The scattering of the $n_v = 0$ volume field into the surface field is described

$$2\pi {r_0}^2 N_v' \left(\underline{H}_{q,\tau}^{*,v}(r_0) \underline{H}_{q,\tau}^{v}(r_0) \sum_{n_v} A_{n_v}(z) + \frac{\Delta r}{4 r_0} \underline{H}_{q,\tau}^{*,v}(r_0) \underline{H}_{q,\tau}^{s} \sum_{n_s} B_{n_s}(z) \left(e^{i\bar{k}_z z(1-n_v+n_s)} + e^{i\bar{k}_z z(-1-n_v+n_s)} \right) \right) \qquad (7)$$

For a non-zero result after integrating, the conditions $1 - n_v + n_s = 0\,; n_s^1 = n_v - 1$ and $-1 - n_v + n_s = 0; n_s^2 = n_v + 1$ must hold true demonstrating the potential for coupling of the fundamental volume field and $n_s \pm 1$ surface field harmonics. Likewise, scattering between the $n_v \pm 1$ and $n_s = 0, \pm 2$ harmonics is also possible. Scattering of the surface field into the volume field is investigated in a similar manner, multiplying Eq.(5) by $e^{-i\bar{k}_z z n_s}$. Expanding and neglecting the same terms as before gives the following expression after integration:

$$2\pi {r_0}^2 N_s' \left(\frac{\Delta r}{4r_0} \left(e^{i\bar{k}_z z(1-n_s+n_v)} + e^{-i\bar{k}_z z(1+n_s-n_v)} \right) \underline{H}_{q,\tau}^{*,s}(r_0) \underline{H}_{q,\tau}^{v}(r_0) \sum_{n_v=-\infty}^{\infty} A_{n_v}(z) + \frac{1}{2} \underline{\overline{H}}_{q,\tau}^{*,s}(r_0) \underline{H}_{q,\tau}^{s}(r_0) \sum_{n_s} B_{n_s}(z) \right) \tag{8}$$

This expression is comprised of two parts, the first defining scattering of the surface field into the volume field and the second describing the accumulation of a localized surface field (which has a dissipative effect and does not contribute to the coupling of volume and surface fields). Once again, to eliminate the exponential terms and obtain a non-zero result, the following conditions must be met: $1 - n_s + n_v = 0\,;\, n_v^1 = n_s - 1$ and $1 + n_s - n_v = 0\,;\, n_v^2 = n_s + 1$. Coupling coefficients are introduced to describe the mutual resonant scattering (i.e. the volume field scattering into the surface field $\alpha_{v,s}$ and the surface field scattering into the volume field $\alpha_{s,v}$) leading to the following set of coupled wave equations.

$$\nabla_z^2 C_q^s(z) - \omega\hat{\delta} C_q^s(z) + \frac{\overline{\omega}_0 \Delta}{c^2} C_q^s(z) = N_s \oint \underline{j}_m \underline{H}_{q'}^* \, d\sigma \tag{9a}$$

$$\frac{\partial^2 A_n(z)}{\partial z^2} - 2i(n)\bar{k}_z \frac{\partial A_n(z)}{\partial z} - \bar{k}_z(n)^2 A_n(z) + \left(\omega\hat{\delta} + \frac{\overline{\omega}_0 \Delta}{c^2}\right) A_n(z) = \alpha_{v,s}\big(B_{n-1}(z) + B_{n+1}(z)\big) \tag{9b}$$

$$\frac{\partial^2 B_n(z)}{\partial z^2} + 2i\bar{k}_z \frac{\partial B_n(z)}{\partial z} - {\bar{k}_z}^2 B_n(z) + \left(\frac{\overline{\omega}_0 \Delta}{c^2} - \omega\hat{\delta}\right) B_n(z) = \alpha_{s,v}\big(A_{n-1}(z) + A_{n+1}(z)\big) \tag{9c}$$

Combining these coupling coefficients into a single parameter, we define $\alpha = \sqrt{\alpha_{v,s}\alpha_{s,v}}$. Finally, new amplitude constants, $\tilde{A}_{n_v}(z) = A_{n_v}(z)\sqrt{\alpha_{s,v}}/\sqrt{\alpha_{v,s}}$ and $\tilde{B}_{n_s}(z) = B_{n_s}(z)\sqrt{\alpha_{v,s}}/\sqrt{\alpha_{s,v}}$ are introduced to give the following normalized coupled wave equations:

$$\frac{\partial^2 \tilde{A}_n(z)}{\partial z^2} - 2i(n)\bar{k}_z \frac{\partial \tilde{A}_n(z)}{\partial z} - \bar{k}_z(n)^2 \tilde{A}_n(z) + \left(\omega\hat{\delta} + \frac{\overline{\omega}_0 \Delta}{c^2}\right) \tilde{A}_n(z) = \alpha\big(B_{n-1}(z) + B_{n+1}(z)\big) \tag{10a}$$

$$\frac{\partial^2 \tilde{B}_n(z)}{\partial z^2} + 2i\bar{k}_z \frac{\partial \tilde{B}_n(z)}{\partial z} - {\bar{k}_z}^2 \tilde{B}_n(z) + \left(\frac{\overline{\omega}_0 \Delta}{c^2} - \omega\hat{\delta}\right) \tilde{B}_n(z) = \alpha\big(A_{n-1}(z) + A_{n+1}(z)\big) \tag{10b}$$

where the normalized coupling coefficient α is defined as,

$$\alpha = \frac{\pi r_0 N_v' N_s' \Delta r}{2} \sqrt{\left(\underline{H}_{q,\tau}^{*,v}(r_0)\underline{H}_{q,\tau}^{s}(r_0)\right)\left(\underline{H}_{q,\tau}^{*,s}(r_0)\underline{H}_{q,\tau}^{v}(r_0)\right)} \tag{11}$$

Solving Eq.(12) involves performing an integral mode calculation around the cylindrical cross section. Analytical dispersion diagrams can otherwise be obtained by treating α and Γ as variable parameters and solving the following coupled dispersion equation:

$$\begin{gathered}(\omega_e^2 - \Lambda^2)[\Lambda^4 - 2\Lambda^2(2 + \Gamma^2 + \omega_e^2) + (2 - \Gamma^2 + \omega_e^2)^2] \\ = 2\alpha^4(2 - \Gamma^2 + \omega_e^2 - \Lambda^2)\end{gathered} \tag{12}$$

where Λ is the normalised wave vector, $\omega_e = \sqrt{\delta^2 + 2\delta + \tilde{\Delta}^2}$ is a variable angular frequency and $\delta = (\omega - \Omega)/\Omega$, $\tilde{\Delta} = \Phi/\Omega$, $\Gamma = 2\bar{k}_z c/((\omega_0^v)^2 + (\omega_0^s)^2)$ are renormalized detuning parameters with constants $\Phi, \Omega = \sqrt{(\omega_0^s)^2 \mp (\omega_0^v)^2/2}$.

Using the above equations, analytical scoping calculations provided the starting parameters that were then used in the numerical modelling, described in the following section 4, which then resulted in determining the dimensions used in the construction of the interaction structure that was used in the experiment reported in section 5.

4. Numerical modelling

Numerical modelling of the electromagnetic field evolution and eigenmode excitation has been conducted using the 3D code MAGIC to help to design the interaction structure and to improve understanding of the experimental measurements. The 3D modelling of such structures is a challenge due to the large variation of the geometrical parameters (dimensions) and the oversized nature of the lattice structure. To optimise the use of the computer memory and the computer performance a square wave approximation was applied in the case of the low contrast model, while a sinusoidal corrugation has been used to simulate the high contrast lattices. To compare the profiles of the lattices in figures 4.1.(a) and 4.1.(b) the *r-z* cross-sections of the high and low contrast structures (left and right columns respectively) are shown. The inserts in these figures show the typical contour plots of the azimuthal magnetic component B_φ of the eigenfield,

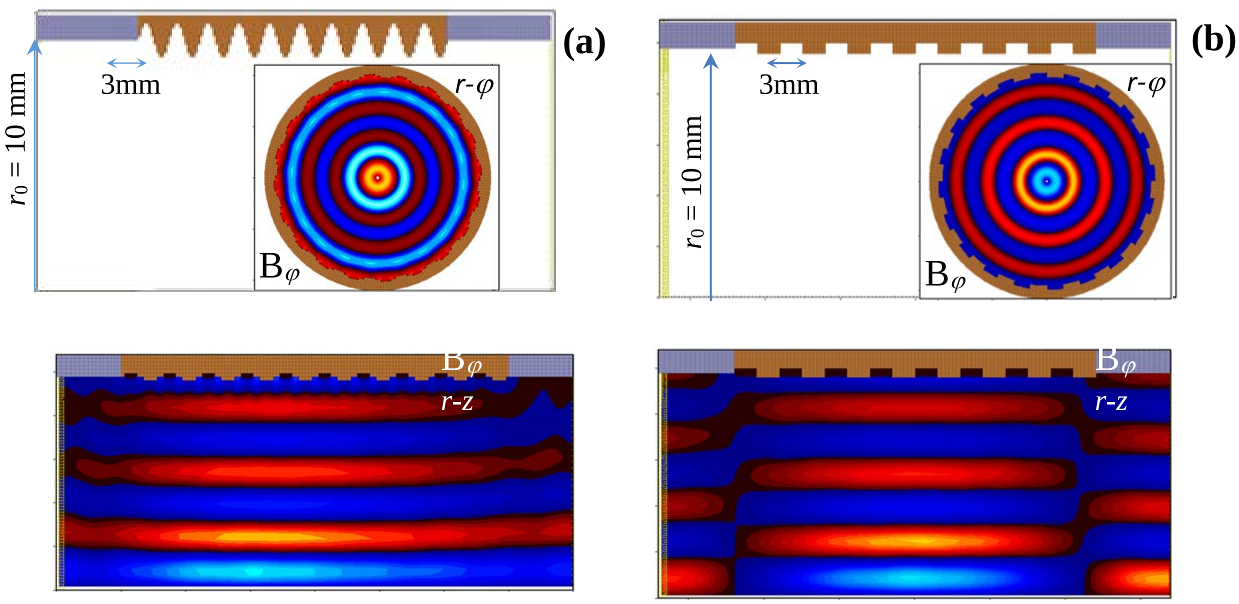

Figure 4.1 Numerical models of the (a) high and (b) low contrast 2D PSLs showing r-z cross-sections of the structures and contour plots of the eigenmodes' azimuthal magnetic field component excited, in r-φ (insert to the first figure) and r-z (second figure)

CST Microwave Studio and CST Particle Studio have also been used to model the 2D PSL structure and the electron beam excitation of the highly overmoded interaction structure.

5. Experiments

The parameters of the magnetic field solenoid used in the experiments are shown in the table below

Magnetic Field Range	1.65 - 2.1 T
Layers	14
Turns/layer	103
Average Diameter	5.68 cm
Wire size	2.2 x 2.2 mm
Length of wire	285.25 m

Table of parameters of the cavity magnetic field solenoid.

The cylindrical 2D PSL structure is described by equation (5.1)

$$r = r_0 + \Delta r\, cos(k_z z) \cos(m\emptyset) \tag{5.1}$$

where r_0 is the radius of the unperturbed waveguide, Δr is the amplitude of the corrugation, $k_z=2\pi/d_z$, where d_z is the period of the corrugation over the z - coordinate and m is the number of azimuthal variations of the corrugation.

(a) (b)

Fig. 5.1 Examples of metallic periodic surface lattice enhanced cavities (a) copper cavity constructed using electrodeposition on an aluminum mandrel (b) silver/chromium alloy cavity manufactured by a casting process using a 3D printed pattern to create the mold.

In our case the 3D printing procedure is a two stage process. The first stage involves creating a wax former to the 10's of microns precision and then using this former to create a mold for the component, where the silver – chromium molten alloy is deposited.

Fig. 5.2. Fully assembled experiment, showing e-beam gun, solenoid and output waveguide and output window, with the cable pulser in the background.

A Faraday cup, a metal cup was used to collect the current of the electrons in the beam. The impacting electrons transferred a current onto a tap off resistor where the voltage drop across the tap off resistor was measured using a digital storage oscilloscope. The design of the specially shaped Faraday cup minimized the number of secondary electrons emitted to avoid increased errors in the measurement of the current. Due to the current induced in the Faraday cup this had to be separated from the other parts of the experiment with an insulator to ensure the current flowed through the current measuring resistor. There were two 100 ohm resistors that connected the Faraday cup to the beam tube of the experiment which was grounded with a 10 ohm tap off resistor at the bottom connected to a digital oscilloscope. The current measured by the Faraday cup then passed through the resistor to earth while the oscilloscope connected to the bottom resistor measured the voltage across it, which was further attenuated by the insertion of a 30dB in-line attenuator.

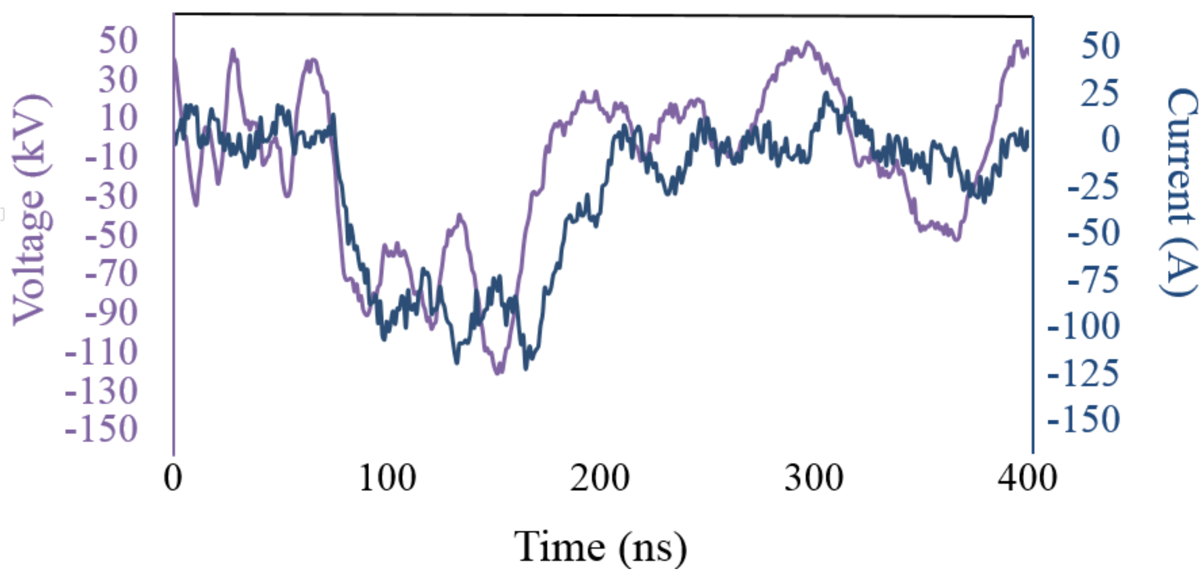

Fig. 5.3 The beam current and accelerating voltage seen at the cathode. A value of 80 kV produced a current of approximately 100 A.

The experiment was operated in single-pulse mode and the microwave receiver system, screened in a metal box, was composed of a small microwave receiving horn followed by attenuators and a Flann microwave detector. Power levels were measured by the W-band Flann rectifying crystal detector, which essentially rectified the millimeter wave signal to produce a voltage output, which was then recorded on an oscilloscope. The measured output was 134 kW. The frequency spectrum of the output was analysed using a series of high pass cut-off filters. Fig. 5.4 demonstrates that the millimeter wave output lies between ~80 GHz and 85 GHz.

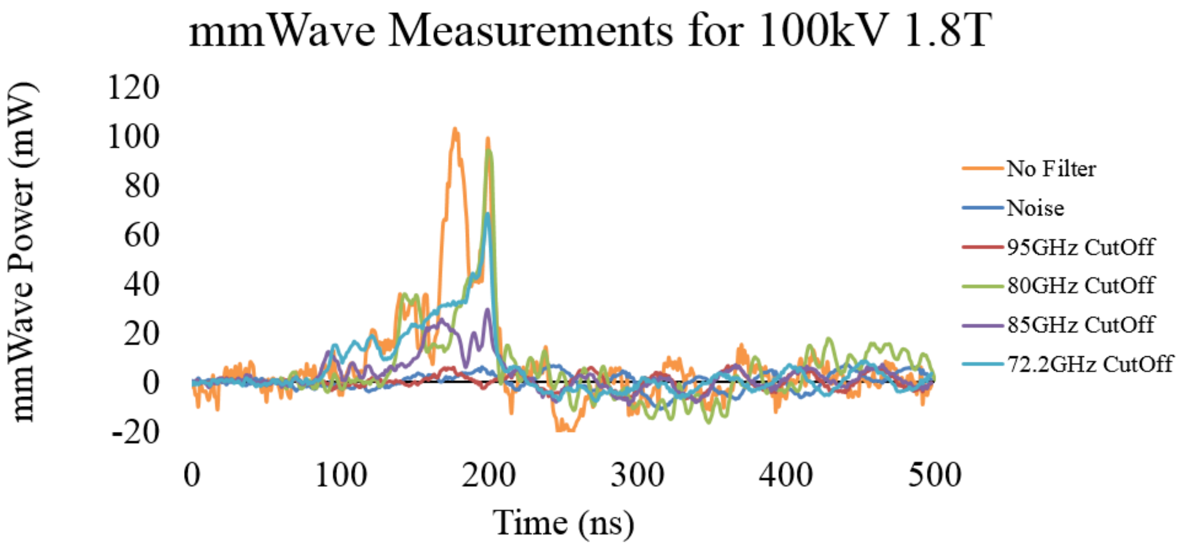

Fig. 5.4. The power produced in the presence of a particular cut – off filter. Light blue line 70 GHz, Green line – 75 GHz, Purple line 80 GHz, red line 85 GHz dark blue line 95 GHz. It is noted that using a 85 GHz cut – off filter results in no mm wave output at all with output measured for cut-off filters above 80 GHz indicating that the signal lies below 85 GHz.

6. Conclusions

During the project the work completed included the study of 2D PSLs using analytical theory, numerical modelling, component design, construction and operation of an experiment. Methods of manufacture of the 2D PSLs included electrodeposition and 3D printing. An output power of 134 kW at a frequency of ~83GHz was measured in a highly overmoded experiment. Although millimeter-wave output was successfully measured the efficiency of between 1% and 2% was significantly lower than expected but the reasons for this are understood.

The concept of using 2D PSLs to enhance high-power microwave and millimeter-wave sources has demonstrated its validity and future work will be aimed at fully realizing the potential of this concept. An improved experiment is presently underway supported by the new AFOSR award FA9550-17-1-0095 that started 15 April 2017. The electron beam used to excite the 2D PSL structure is being upgraded in two ways. The component of the perpendicular velocity in the electron beam is being reduced and the beam is being propagated closer to the 2D PSL structure. The guide solenoidal magnetic field has also been designed to be stronger. It is planned that the D/λ ratio will be increased in later experiments. The diagnostics of the millimeter-wave output are at the same time being improved. Instead of the filter method of estimating the frequency, a heterodyne technique is being brought into use, in order to more precisely measure the output frequency.

7. Publications

[1] Phipps, A.R., MacLachlan, A.J., Robertson, C.W., Zhang, L., Konoplev, I.V., Cross, A.W. and Phelps, A.D.R. "Electron beam excitation of coherent sub-terahertz radiation in periodic structures manufactured by 3D printing," Nuclear Instruments and Methods in Physics Research, Section B: Beam Interactions with Materials and Atoms, vol. 402, pp. 202-205 (2017).
[2] Phelps, A. D. R. Progress in Microwave to Sub-Thz Sources at Strathclyde. vol. 149. EPJ Web of Conferences, (2017).

Conference papers:
[3] Phipps, A. R., MacLachlan, A. J., Robertson C. W., Konoplev, I. V., Phelps, A. D. R. and Cross, A. W., "Numerical simulation and experimental design of a mm-wave BWO utilising a structurally-induced surface field", UK National Vacuum Electronics Conference, NVEC, London, June 2013.
[4] Phipps, A. R., MacLachlan, A. J., Robertson, C. W., Konoplev, I. V., Phelps, A. D. R., and Cross, A. W. "Numerical analysis and experimental design of a 103 GHz Cherenkov maser", in 39th IEEE International Conference on Infrared, Millimeter, and Terahertz waves (IRMMW-THz), Tucson, Arizona, USA, September 2014.
[5] MacLachlan, A. J., Phipps, A. R., Robertson, C. W., Phelps, A. D. R., Konoplev, I. V., and Cross, A. W.,"Planar periodic surface lattices for use in millimeter-wave sources", ", in 39th IEEE International Conference on Infrared, Millimeter, and Terahertz waves (IRMMW-THz), Tucson, Arizona, USA, September 2014.
[6] Phipps, A.R., MacLachlan, A.J., Robertson, C.W., Konoplev, I.V., Ronald, K., Cross, A.W., Whyte, C.G., Phelps, A.D.R., "Cherenkov maser experiments based on a 2D Periodic Surface Lattice", IEEE International Conference on Plasma Sciences (ICOPS), 24-28 May, 2015, Antalya, Turkey,
[7] Phelps, A.D.R., "Recent progress in HPM research", DEPS UK/US Directed Energy Workshop, 15-19 June, 2015, Swindon, UK.
[8] MacLachlan, A.J., Phipps, A.R., Robertson, C.W., Cross, A.W, Konoplev, I.V., and Phelps, A.D.R., Periodic Surface Lattice Modelling and Experiments, 14-16 September, UCMMT 2015, Cardiff, UK.
[9] MacLachlan, A.J., Phipps, A.R., Robertson, C.W., Konoplev, I.V., Cross, A.W, and Phelps, A.D.R., "Periodic Surface Lattice Experiments", 18 November, NVEC 2015, Glasgow, UK.
[10] MacLachlan, A. J., A. R. Phipps, C. W. Robertson, A. W. Cross, I. V. Konoplev, and A. D. R. Phelps. Periodic Surface Lattice Modelling and Experiments. 2015 8th UCMMT 2015..

Invited Lectures, Presentations, Talks:
[11] Phipps, A.R., "Millimetre - Wave Backward Wave Oscillator Incorporating a Structurally Induced Surface Field", Presentation over the internet to the AFOSR MURI Consortium on Transformational Electromagnetics, Chaired by Edl Schamiloglu, UNM, USA, June 28, 2013.
[12] Phelps, A.D.R., "High Power Microwave Low-Contrast Surface Artificial Materials", Plasma and Electroenergetics Program Review, 18-19 December, 2014, BRICC, Arlington,

VA, USA.
[13] Phipps, A.R., “2D Periodic surface lattice Cherenkov maser experiment”,10 April, 2015, Presentation over the internet to the AFOSR MURI Consortium on Transformational Electromagnetics, Chaired by Edl Schamiloglu, UNM, USA.
[14] Cross, A.W., “2D Periodic Surface Lattice Backward Wave Oscillator Experiment”, 4 December, 2015, Presentation over the internet to the AFOSR MURI Consortium on Transformational Electromagnetics, Chaired by Edl Schamiloglu, UNM, USA.
[15] MacLachlan, A.J., “Two dimensional periodic surface lattices” 4 seminars presented in USA during Fall of 2016, under WoS program, 2016.
[16] Phelps, A.D.R., “High-power millimeter-wave sources”, ICOPS Atlantic City, USA, May 2017 (invited plenary).

Two postgraduate research students: A.J. MacLachlan and A.R. Phipps graduated during the period of this award with PhD degrees that were based on research associated with this report.

8. Professional Activities of Principal Investigator: Alan Phelps & Co-Investigators: Adrian Cross and Kevin Ronald (conference and society committees, awards):

Alan Phelps:
Executive committee member of UK IET RF & Microwave TPN (2012 - 2014)
Co-chair of International Advisory Committee, UCMMT conference (2012-2017)
Organizing committee for NVEC 2015 conference
American Physical Society, Plasma Physics Division, Fellowship Election Committee 2016
IEEE Plasma Science and Applications (PSAC) Award 2017
Organizing committee (Treasurer) for ESCAMPIG 2018
International Committee, ICOPS 2018 , Denver USA.

Adrian Cross
Chair of Organizing Committee for NVEC 2015 conference
Technical Area Coordinator for Microwave Generation and Plasma Interactions, ICOPS 2015, Belek, Antalya, Turkey, May , 2015.
Cockcroft Institute Management Committee, 2017-2018

K. Ronald
Co-chair of organizing committee for IPELS 2015 conference